JOURNAL OF THERMOPHYSICS AND HEAT TRANSFER
Vol. 25, No. 2, April–June 2011

Effects of Corrugated Roughness on Gaseous Slip Flow Forced Convection in Microtubes

Arman Sadeghi,* Hassan Salarieh,† Mohammad Hassan Saidi,‡ and Ali Asghar Mozafari§
Sharif University of Technology, 11155-9567 Tehran, Iran

DOI: 10.2514/1.51797

Because of technological restrictions, it is actually impossible to fabricate smooth microchannels. Therefore, exploring the roughness effects on the flow characteristics at microscale is of great importance for scientific communities. The present investigation deals with the effects of corrugated roughness on the fully developed slip flow forced convection in micropipes. The governing equations subject to first-order slip boundary conditions are solved by means of the straightforward perturbation method. Closed-form expressions are obtained for the dimensionless velocity and temperature distributions, for the friction coefficient and pressure drop, and finally for the Nusselt number. The results demonstrate that the corrugated roughness increases both the pressure drop and the heat transfer rate, with the amount of the increase in the pressure drop being a little more. Despite increasing the heat transfer rate, the effect of roughness is found to be unfavorable as it leads to smaller values of the channel performance, defined as the ratio of the heat transfer rate to the pressure drop. In other words, for a given heat transfer rate some increase in pumping power requirements is incurred.

Nomenclature

A	=	channel area, m^2
c_p	=	specific heat at constant pressure, $kJ\,kg^{-1}\,K^{-1}$
D_h	=	hydraulic diameter of channel, $=4A/P$
e_r	=	unit vector in the radial direction
e_θ	=	unit vector in the angular direction
f	=	Fanning friction factor, $2\tau_{w,\mathrm{av}}/\rho U^2$
F_m	=	momentum accommodation coefficient
F_t	=	thermal accommodation coefficient
h	=	heat transfer coefficient, $Wm^{-2}\,K^{-1}$
Kn	=	Knudsen number, $=\lambda/R$
k	=	thermal conductivity, $Wm^{-1}\,K^{-1}$
L	=	characteristic length scale, m
M	=	number of corrugations
Nu	=	Nusselt number, $=hD_h/k$
n	=	normal direction exiting the wall, m
P	=	perimeter, m
Pr	=	Prandtl number, $=\nu/\alpha$
p	=	pressure, Pa
Q	=	total flow rate, $m^3\,s^{-1}$
Q'	=	heat transfer rate per unit length, $W\,m^{-1}$
q	=	wall heat flux, $W\,m^{-2}$
R	=	nominal radius of the channel, m
$\mathcal{R}$	=	gas constant
Re	=	Reynolds number, $=UD_h/\nu$
r	=	radial coordinate, m
r_m	=	maximum r at each θ, $=R+R\varepsilon\sin(M\theta)$
T	=	temperature, K
U	=	mean velocity, $m\,s^{-1}$
u	=	axial velocity, $m\,s^{-1}$
z	=	axial coordinate, m
α	=	thermal diffusivity, $m^2\,s^{-1}$
γ	=	heat capacity ratio
ε	=	relative roughness
η	=	channel performance, WPa^{-1}
θ	=	angular coordinate, rad
λ	=	gas mean free path, m
μ	=	dynamic viscosity, $kgm^{-1}\,s^{-1}$
ν	=	kinematic viscosity, $m^2\,s^{-1}$
ρ	=	density, kgm^{-3}
τ	=	shear stress, Nm^{-2}

Subscripts

av	=	average
b	=	bulk
s	=	fluid properties at solid surface
w	=	wall

Superscript

$*$	=	dimensionless variable

Received 28 July 2010; revision received 23 October 2010; accepted for publication 23 October 2010.

*Ph.D. Student, School of Mechanical Engineering; armansadeghi@mech.sharif.edu.
†Assistant Professor, School of Mechanical Engineering; salarieh@sharif.edu.
‡Professor, School of Mechanical Engineering; saman@sharif.edu.
§Professor, School of Mechanical Engineering; mozafari@sharif.edu.

I. Introduction

THROUGHOUT the past two decades, microelectro mechanical systems (MEMS) have been one of the major advances of industrial technologies because of their lower cost in spite of supplying higher performance. MEMS covers micron-sized, electrically and/or mechanically driven devices. Having been derived initially from the integrated circuit (IC) fabrication technologies, MEMS devices are already emerging as products in both commercial and defense markets such as automotive, aerospace, medical, industrial process control, electronic instrumentation, office equipment, appliances, and telecommunications. Current products include airbag crash sensors, pressure sensors, inkjet printer heads, lab-on-a-chip devices, etc.

Design and optimization of microdevices usually involve the analysis of gas flow through microchannels as an important part of these devices. Because of significant rarefaction effects, the flow physics of gas flow at microscale is quite different from macroscale. The features of this difference, which has been justified by a lot of experiments [1–6], include discontinuities of velocity and temperature on the boundary, non-Newtonian components of stress tensor, non-Fourier heat flux and formation of Knudsen boundary layer [7]. Based on the degree of rarefaction, some of the aforementioned features are present. The degree of rarefaction is measured by the Knudsen number defined as $Kn=\lambda/L$, with L denoting the

characteristic length scale of the device and λ being the mean free path of the gas molecules. The mean free path is given by $\lambda = \mu\sqrt{\pi/2\mathcal{R}T\rho^2}$, where μ is the dynamic viscosity, $\mathcal{R}$ is the gas constant, and T and ρ are the temperature and density of the gas, respectively. Based on a classification given by Beskok and Karniadakis [8], gas flow can be categorized into four regimes according to its Knudsen number. For $Kn < 10^{-3}$, the gas is considered as a continuum, while for $Kn > 10$ it is considered as a free molecular flow. In the Knudsen number ranging between 10^{-3} and 10, two different regimes exist, namely slip flow for $10^{-3} \leq Kn \leq 0.1$ and transition flow for $0.1 < Kn \leq 10$. In the slip flow regime, deviations from the state of continuum are relatively small and the Navier–Stokes equations are still valid, except at the region next to the boundary which is known as Knudsen boundary layer. The Knudsen boundary layer is significant only up to distances of the order of 1 mean free path from the wall [9]. So besides velocity and temperature discontinuities at the wall, its effects are negligible in slip flow regime and the Navier–Stokes equations may be applied to the whole domain. The velocity and temperature discontinuities are incorporated into the solution as boundary conditions. Several forms of the slip boundary conditions have been proposed in the literature, among them first- and second-order slip boundary conditions (based on Knudsen number). Although the second-order slip boundary conditions are more accurate than the first-order conditions, however, the first-order conditions are sufficiently accurate in the slip flow regime [9]. This, accompanied by their simplicity to use, has led to the wide use of the first-order slip boundary conditions in the literature. It is noteworthy that the measured friction factors obtained by Harley et al. [1], Araki et al. [2], Arkilic et al. [4], and Liu et al. [5] matched well with theoretical predictions assuming fully developed first-order slip flow.

Hydrodynamic aspects of slip flow in the circular tube and parallel plate channel were studied by Kennard [10]. Ebert and Sparrow [11] have determined the velocity distribution and pressure drop of slip flow in rectangular and annular ducts. More recently, Duan and Muzychka [12] performed an analytical analysis to describe fully developed laminar flow in elliptical microchannels. They also developed simple approximate models for predicting the friction factor in noncircular microducts at fully developed conditions [13] and in the entrance region [14] as well. All the results in [10–14] show that rarefaction effect decreases pressure drop in microchannels compared with conventional channels for a given mass flow rate.

Aydin and Avci [15,16] studied fully developed laminar slip flow forced convection in a micropipe and microchannel between two parallel plates. The thermally developing cases have been studied by Jeong and Jeong [17,18] by taking the effects of viscous dissipation and streamwise conduction into account. Sadeghi et al. [19] have performed a boundary layer analysis for simultaneously developing flow through parallel plate microchannels. The effects of Knudsen number on friction factor, Nusselt number, and entry length have been determined. Fully developed laminar slip flow forced convection in a rectangular microchannel under H_2 type boundary condition was studied by Tunc and Bayazitoglu [20], using an integral transform method. Thermally developing forced convection in rectangular microchannels for both boundary conditions of constant wall temperature and constant wall heat flux has been studied by Yu and Ameel [21,22], by applying a modified generalized integral transform technique to solve the energy equation, assuming hydrodynamically fully developed flow. Naterer [23] developed a new technique of adaptively optimized microgrooves in a surface, with geometrical profiles selected to minimize entropy production over the surface. Analytical solutions for hydrodynamic and thermal features of fully developed slip flow forced convection in microchannel heat sinks were presented by Khan and Yovanovich [24]. In a recent study, Sadeghi and Saidi [25] examined heat transfer characteristics of fully developed laminar rarefied gas flow in both parallel plate and annular microducts with constant but different wall heat fluxes. They also performed the second law of thermodynamics analysis for slip flow forced convection through two aforementioned geometries [26,27].

All the foregoing studies are dealing with smooth channels. However, because of technological restrictions, it is actually impossible to fabricate smooth microchannels. It is well known that roughness effects do not significantly affect flow characteristics at macroscale due to the fact that at macroscale small values of relative roughness are present. Nevertheless, at microscale we encounter the values of even more that 0.1 for relative roughness [28]. Because of its importance, the roughness effect on liquid flow in microchannel has extensively been investigated in the literature. Experiments were conducted by Peng et al. [29] to investigate the flow characteristics of water flowing through rectangular microchannels having hydraulic diameters of 133–367 μm. The friction behavior of both the laminar and turbulent flows was found to depart from the classical thermofluid correlations. Water flow through microtubes with diameters ranging from 50 to 254 μm was investigated experimentally by Mala and Li [30]. The experimental results indicated that for microtubes with smaller diameters the pressure drop is higher than the predictions of the conventional theory. Wu and Cheng [31] performed an experimental investigation on the laminar convective heat transfer and pressure drop of water in 13 different trapezoidal silicon microchannels. It was found that the Nusselt number and friction coefficient increase with the increase of surface roughness and surface hydrophilic property. Systematic experiments were conducted by Kandlikar et al. [32] using saw-tooth roughness elements in rectangular flow channels. Their efforts resulted in introducing some new parameters including constricted flow diameter, the nominal channel diameter minus 2 times of average roughness height. They recommended the use of the constricted flow diameter instead of the nominal diameter in obtaining flow characteristics in microchannels.

Surface roughness on channel walls introduces surface-fluid interactions that are not well defined and cannot be easily handled through analytical or numerical treatments. Nevertheless, some attempts have been performed to theoretically investigate roughness effects on gas flow in microchannels. Li et al. [33] proposed a model that describes the behavior of rarefied gas flow in long microtubes. The rough surface was modeled as an annulus porous film pressed on an impermeable surface. Sun and Faghri [34] investigated the effects of surface roughness on nitrogen flow in a microchannel using direct simulation Monte–Carlo method. The surface roughness was modeled by an array of rectangular modules placed on one side of a parallel plate channel. It was revealed that as the relative roughness increases the friction factor increases. The results also showed that the effect of surface roughness is more pronounced at low Knudsen numbers. In two recent studies, Duan and Muzychka [35,36] considered the effects of corrugated roughness in both angular and axial directions of micropipes on pressure drop of the gas flow. The governing equations were solved by means of the perturbation method using first-order slip boundary condition. The developed models show a significant increase in pressure drop due to roughness.

Unlike hydrodynamic features, the roughness effects on heat transfer features in rarefied flow through microchannels have rarely been investigated. The aim of the present work is to study the effects of corrugated roughness on the heat transfer characteristics of the fully developed forced convection of a rarefied gas flow through micropipes in slip flow regime. The classical boundary condition of H_1 type is considered which refers to constant wall heat flux in the axial direction, but having constant wall temperature in the peripheral direction at any cross section. This boundary condition may apply to the channels constructing from highly conductive materials such as copper and aluminum [37]. The governing equations along with first-order slip boundary conditions are solved by means of the perturbation method. Approximate analytical solutions are obtained for the dimensionless velocity and temperature distributions, for the pressure drop and friction coefficient and finally for the Nusselt number.

II. Slip Velocity and Temperature Jump

As stated before, because of rarefaction effects, the velocity and temperature of the gas at the solid surface are different from the

corresponding values of the wall. The velocity of the gas at the wall is known as the slip velocity and the difference between the wall temperature and the gas temperature at the wall is known as the temperature jump. The first-order boundary conditions for velocity and temperature at the solid surface may be written as [38]

$$u_s = \frac{2 - F_m}{F_m}\lambda\left(\frac{\partial u}{\partial n}\right)_w \tag{1}$$

$$T_s - T_w = \frac{2 - F_t}{F_t}\frac{2\gamma}{1+\gamma}\frac{\lambda}{Pr}\left(\frac{\partial T}{\partial n}\right)_w \tag{2}$$

where u_s and T_s are the velocity and temperature of the gas at the wall, respectively, T_w is the wall temperature, Pr is the Prandtl number, γ is the heat capacity ratio, n is the inward normal direction to the wall, F_m is the tangential momentum accommodation coefficient, and F_t is the thermal accommodation coefficient. Even though different parameters that affect surface interaction, such as the magnitude and the direction of the velocity, may affect the value of accommodation coefficients, however, these coefficients are reasonably constant for a given gas and surface combination [39]. As noted by Hadjiconstantinou [9], for most engineering applications the values of accommodation coefficients are close to unity.

III. Problem Formulation

Consider slip flow forced convection through a circular micropipe. The flow is considered to be hydrodynamically and thermally fully developed, steady, laminar and having constant thermophysical properties. The flow velocities are considered to be low enough to allow neglecting the viscous dissipation and compressibility effects. It is assumed that, due to manufacturing defects, the channel possesses a rough surface which may be described approximately by the sinusoidal function $r = R + R\varepsilon\sin(M\theta)$ as shown in Fig. 1, where R is the nominal radius of the channel, M is the number of corrugations and ε is the relative roughness. The thermal boundary condition is assumed to be the constant wall heat flux of the first kind, H_1.

A. Hydrodynamic Features

The momentum equation at fully developed condition is given by

$$\nabla^2 u = \frac{1}{\mu}\frac{\mathrm{d}p}{\mathrm{d}z} \tag{3}$$

in which z is the axial coordinate and

$$\nabla^2 = \frac{\partial^2}{\partial r^2} + \frac{1}{r}\frac{\partial}{\partial r} + \frac{1}{r^2}\frac{\partial^2}{\partial\theta^2} + \frac{\partial^2}{\partial z^2} \tag{4}$$

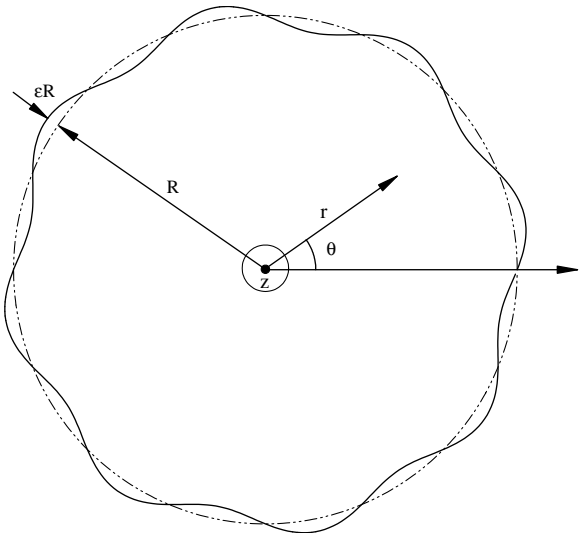

Fig. 1 Geometry of the physical problem and coordinate system.

Since for fully developed flow $u = u(r,\theta)$, therefore, $\partial^2 u/\partial z^2 = 0$. The momentum equation is constrained by the following boundary conditions

$$u \neq \infty \quad \text{at } r = 0 \tag{5}$$

$$u = \beta_m\lambda\frac{\partial u}{\partial n} \quad \text{at } r = R + R\varepsilon\sin(M\theta) \tag{6}$$

which for brevity the parameter $\beta_m = (2 - F_m)/F_m$ has been used. To generalize the results, the momentum equation along with the corresponding boundary conditions are written in the following dimensionless forms

$$\nabla^{*2}u^* = \frac{\partial^2 u^*}{\partial r^{*2}} + \frac{1}{r^*}\frac{\partial u^*}{\partial r^*} + \frac{1}{r^{*2}}\frac{\partial^2 u^*}{\partial\theta^2} = \frac{R^2}{\mu U}\frac{\mathrm{d}p}{\mathrm{d}z} \tag{7}$$

$$u^* \neq \infty \quad \text{at } r^* = 0 \tag{8}$$

$$u^* = \beta_m Kn\frac{\partial u^*}{\partial n^*} \quad \text{at } r^* = 1 + \varepsilon\sin(M\theta) \tag{9}$$

in which $r^* = r/R$, $Kn = \lambda/R$, $\nabla^{*^2} = R^2\nabla^2$, and $u^* = u/U$ with U being the mean velocity. The next step of the procedure is finding $\partial u^*/\partial n^*$ at the wall. From the calculus, n^* may be expressed as follows

$$n^* = \frac{-\nabla^*[r^* - 1 - \varepsilon\sin(M\theta)]}{|\nabla^*[r^* - 1 - \varepsilon\sin(M\theta)]|} = -\frac{e_r - \frac{M\varepsilon}{r^*}\cos(M\theta)e_\theta}{\sqrt{1 + \frac{M^2\varepsilon^2}{r^{*2}}\cos^2(M\theta)}}$$
$$\text{at } r^* = 1 + \varepsilon\sin(M\theta) \tag{10}$$

where e_r and e_θ are the unit vectors in the radial and angular directions, respectively. The dimensionless velocity gradient at the boundary is thus

$$\frac{\partial u^*}{\partial n^*} = \nabla^* u^*\cdot n^* = -\left(\frac{\partial u^*}{\partial r^*}e_r + \frac{1}{r^*}\frac{\partial u^*}{\partial\theta}e_\theta\right)$$
$$\cdot\frac{e_r - \frac{M\varepsilon}{r^*}\cos(M\theta)e_\theta}{\sqrt{1 + \frac{M^2\varepsilon^2}{r^{*2}}\cos^2(M\theta)}} = -\frac{\frac{\partial u^*}{\partial r^*} - \frac{M\varepsilon}{r^{*2}}\cos(M\theta)\frac{\partial u^*}{\partial\theta}}{\sqrt{1 + \frac{M^2\varepsilon^2}{r^{*2}}\cos^2(M\theta)}} \tag{11}$$

Therefore, the boundary condition (9) may be rearranged as

$$u^*\sqrt{1 + \frac{M^2\varepsilon^2}{r^{*2}}\cos^2(M\theta)} = -\beta_m Kn\left[\frac{\partial u^*}{\partial r^*} - \frac{M\varepsilon}{r^{*2}}\cos(M\theta)\frac{\partial u^*}{\partial\theta}\right]$$
$$\text{at } r^* = 1 + \varepsilon\sin(M\theta) \tag{12}$$

or

$$u^*\left[1 + \frac{M^2\varepsilon^2}{2r^{*2}}\cos^2(M\theta) + \cdots\right]$$
$$= -\beta_m Kn\left[\frac{\partial u^*}{\partial r^*} - \frac{M\varepsilon}{r^{*2}}\cos(M\theta)\frac{\partial u^*}{\partial\theta}\right] \quad \text{at } r^* = 1 + \varepsilon\sin(M\theta) \tag{13}$$

We can expand the terms r^{*-2}, u^*, $\partial u^*/\partial r^*$, and $\partial u^*/\partial\theta$ in Taylor series to obtain

$$r^{*-2} = (1 - \varepsilon\sin(M\theta) + \varepsilon^2\sin^2(M\theta) + \cdots)^2 \tag{14}$$

$$u^*(1 + \varepsilon\sin(M\theta), \theta) = u^*(1,\theta) + \varepsilon\sin(M\theta)\frac{\partial u^*}{\partial r^*}(1,\theta)$$
$$+ \frac{\varepsilon^2}{2}\sin^2(M\theta)\frac{\partial^2 u^*}{\partial r^{*2}}(1,\theta) + \cdots \tag{15}$$

$$\frac{\partial u^*}{\partial r^*}(1+\varepsilon\sin(M\theta),\theta)=\frac{\partial u^*}{\partial r^*}(1,\theta)+\varepsilon\sin(M\theta)\frac{\partial^2 u^*}{\partial r^{*2}}(1,\theta)+\frac{\varepsilon^2}{2}\sin^2(M\theta)\frac{\partial^3 u^*}{\partial r^{*3}}(1,\theta)+\cdots \tag{16}$$

$$\frac{\partial u^*}{\partial \theta}(1+\varepsilon\sin(M\theta),\theta)=\frac{\partial u^*}{\partial \theta}(1,\theta)+\varepsilon\sin(M\theta)\frac{\partial^2 u^*}{\partial r^*\partial\theta}(1,\theta)+\frac{\varepsilon^2}{2}\sin^2(M\theta)\frac{\partial^3 u^*}{\partial r^{*2}\partial\theta}(1,\theta)+\cdots \tag{17}$$

Let us seek an approximate solution in the form of a Poincare type asymptotic expansion for velocity as

$$u^*(r^*,\theta)=u_0^*(r^*,\theta)+\varepsilon u_1^*(r^*,\theta)+\varepsilon^2 u_2^*(r^*,\theta)+\cdots \tag{18}$$

Substituting the above expansion into Eq. (7) and equating the terms having equal powers of ε leads to the following equations for u_0^*, u_1^*, and u_2^*

$$\nabla^{*2}u_0^*=\frac{R^2}{\mu U}\frac{\mathrm{d}p}{\mathrm{d}z},\qquad \nabla^{*2}u_1^*=0,\qquad \nabla^{*2}u_2^*=0 \tag{19}$$

Substituting expansion (18) into Eqs. (15–17), setting the resulting equations along with Eq. (14) into Eq. (13), and equating coefficients of equal powers of ε result in the following boundary conditions

$$u_0^*(1,\theta)=-\beta_m Kn\frac{\partial u_0^*}{\partial r^*}(1,\theta) \tag{20}$$

$$u_1^*(1,\theta)+\sin(M\theta)\frac{\partial u_0^*}{\partial r^*}(1,\theta)=-\beta_m Kn\left[\frac{\partial u_1^*}{\partial r^*}(1,\theta)+\sin(M\theta)\frac{\partial^2 u_0^*}{\partial r^{*2}}(1,\theta)-M\cos(M\theta)\frac{\partial u_0^*}{\partial\theta}(1,\theta)\right] \tag{21}$$

$$\begin{aligned}u_2^*(1,\theta)&+\frac{M^2}{2}\cos^2(M\theta)u_0^*(1,\theta)+\sin(M\theta)\frac{\partial u_1^*}{\partial r^*}(1,\theta)\\&+\frac{\sin^2(M\theta)}{2}\frac{\partial^2 u_0^*}{\partial r^{*2}}(1,\theta)=-\beta_m Kn\left[\frac{\partial u_2^*}{\partial r^*}(1,\theta)\right.\\&+\sin(M\theta)\frac{\partial^2 u_1^*}{\partial r^{*2}}(1,\theta)+\frac{\sin^2(M\theta)}{2}\frac{\partial^3 u_0^*}{\partial r^{*3}}(1,\theta)\\&+2M\sin(M\theta)\cos(M\theta)\frac{\partial u_0^*}{\partial\theta}(1,\theta)-M\cos(M\theta)\frac{\partial u_1^*}{\partial\theta}(1,\theta)\\&\left.-M\sin(M\theta)\cos(M\theta)\frac{\partial^2 u_0^*}{\partial r^*\partial\theta}(1,\theta)\right]\end{aligned} \tag{22}$$

The solution of Eqs. (19) subject to boundary conditions (20–22) is

$$u_0^*=a_0+b_0 r^{*2} \tag{23}$$

$$u_1^*=a_1 r^{*M}\sin(M\theta) \tag{24}$$

$$u_2^*=a_2+b_2 r^{*2M}\cos(2M\theta) \tag{25}$$

with the following coefficients

$$\begin{aligned}a_0&=-\frac{R^2}{4\mu U}\frac{\mathrm{d}p}{\mathrm{d}z}[1+2\beta_m Kn],\qquad b_0=\frac{R^2}{4\mu U}\frac{\mathrm{d}p}{\mathrm{d}z}\\a_1&=-\frac{R^2}{2\mu U}\frac{\mathrm{d}p}{\mathrm{d}z}\frac{1+\beta_m Kn}{1+\beta_m KnM}\\a_2&=\frac{R^2}{\mu U}\frac{\mathrm{d}p}{\mathrm{d}z}\left[\beta_m KnM\left(\frac{M}{8}-\frac{1}{4}\frac{1+\beta_m Kn}{1+\beta_m KnM}\right)+\frac{M}{4}\frac{1+\beta_m Kn}{1+\beta_m KnM}-\frac{1}{8}\right]\\b_2&=\frac{\frac{R^2}{\mu U}\frac{\mathrm{d}p}{\mathrm{d}z}[\beta_m KnM(\frac{M}{8}+\frac{1-2M}{4}\frac{1+\beta_m Kn}{1+\beta_m KnM})-\frac{M}{4}\frac{1+\beta_m Kn}{1+\beta_m KnM}+\frac{1}{8}]}{1+2\beta_m KnM}\end{aligned} \tag{26}$$

The term $(R^2/\mu U)(\mathrm{d}p/\mathrm{d}z)$ may be removed from the velocity distribution invoking the fact that the average dimensionless velocity over the cross section of the channel is equal to unity, that is

$$\frac{\int u^*\,\mathrm{d}A^*}{\int \mathrm{d}A^*}=\frac{\int u^*\,\mathrm{d}A^*}{A^*}=1 \tag{27}$$

The dimensionless channel area A^* is evaluated as

$$A^*=M\int_0^{2\pi/M}\int_0^{1+\varepsilon\sin(M\theta)} r^*\,\mathrm{d}r^*\,\mathrm{d}\theta=\pi\left(1+\frac{\varepsilon^2}{2}\right) \tag{28}$$

and the dimensionless flow rate is given by

$$\int u^*\,\mathrm{d}A^*=M\int_0^{2\pi/M}\int_0^{1+\varepsilon\sin(M\theta)} u^* r^*\,\mathrm{d}r^*\,\mathrm{d}\theta=\pi[a_0+b_0/2+(a_0/2+3b_0/2+a_1+a_2)\varepsilon^2+O(\varepsilon^4)] \tag{29}$$

By substituting the coefficients of velocity distribution into the above equation, and setting the resulting expression accompanied by Eq. (28) into Eq. (27), we come up with the following expression

$$\frac{R^2}{\mu U}\frac{\mathrm{d}p}{\mathrm{d}z}=\frac{1+\frac{\varepsilon^2}{2}}{-\frac{1}{8}-\frac{\beta_m Kn}{2}+[\frac{1}{8}-\frac{\beta_m Kn}{4}-\frac{1}{2}\frac{1+\beta_m Kn}{1+\beta_m KnM}+\beta_m KnM(\frac{M}{8}-\frac{1}{4}\frac{1+\beta_m Kn}{1+\beta_m KnM})+\frac{M}{4}\frac{1+\beta_m Kn}{1+\beta_m KnM}]\varepsilon^2+O(\varepsilon^4)} \tag{30}$$

From the above equation, the pressure gradient for a given mean velocity may be obtained. Both sides of Eq. (30) should be multiplied by $A^{-1}=1/\pi R^2(1+\varepsilon^2/2)$ to obtain the pressure gradient for a given flow rate as follows:

$$\frac{\pi R^4}{\mu Q}\frac{\mathrm{d}p}{\mathrm{d}z}=\frac{1}{-\frac{1}{8}-\frac{\beta_m Kn}{2}+[\frac{1}{8}-\frac{\beta_m Kn}{4}-\frac{1}{2}\frac{1+\beta_m Kn}{1+\beta_m KnM}+\beta_m KnM(\frac{M}{8}-\frac{1}{4}\frac{1+\beta_m Kn}{1+\beta_m KnM})+\frac{M}{4}\frac{1+\beta_m Kn}{1+\beta_m KnM}]\varepsilon^2+O(\varepsilon^4)} \tag{31}$$

in which $Q = UA$ is the total flow rate. One of the important parameters of the hydrodynamics is the friction factor defined as

$$f = \frac{2\tau_{w,\mathrm{av}}}{\rho U^2} = \frac{2(-\frac{A}{P}\frac{\mathrm{d}p}{\mathrm{d}z})}{\rho U^2} \tag{32}$$

with P being the channel cross-section perimeter. It should be mentioned that the average wall shear stress, $\tau_{w,\mathrm{av}}$, has been related to the pressure gradient using an overall momentum balance on an element of the fluid with the length of $\mathrm{d}z$. The final form of the friction factor in the form of Poiseuille number is

$$fRe = \frac{-(1+\frac{\varepsilon^2}{2})\frac{D_h^{*2}}{2}}{-\frac{1}{8}-\frac{\beta_m Kn}{2}+[\frac{1}{8}-\frac{\beta_m Kn}{4}-\frac{1}{2}\frac{1+\beta_m Kn}{1+\beta_m KnM}+\beta_m KnM(\frac{M}{8}-\frac{1}{4}\frac{1+\beta_m Kn}{1+\beta_m KnM})+\frac{M}{4}\frac{1+\beta_m Kn}{1+\beta_m KnM}]\varepsilon^2+O(\varepsilon^4)} \tag{33}$$

in which $D_h^* = 4A^*/P^*$ is the dimensionless hydraulic diameter. Although according to Shah and London [37] the perimeter should be evaluated numerically, however, we may seek an approximate expression for small values of ε. The dimensionless perimeter is given by

$$\begin{aligned} P^* &= M\int_0^{\frac{2\pi}{M}} \sqrt{r_m^{*2}+\left(\frac{\mathrm{d}r_m^*}{\mathrm{d}\theta}\right)^2}\,\mathrm{d}\theta \\ &= M\int_0^{\frac{2\pi}{M}} \sqrt{1+2\varepsilon\sin(M\theta)+\varepsilon^2\sin^2(M\theta)+M^2\varepsilon^2\cos^2(M\theta)}\,\mathrm{d}\theta \end{aligned} \tag{34}$$

It should be pointed out that r_m^* is the maximum value of r^* at each θ, i.e., $r_m^* = 1+\varepsilon\sin(M\theta)$. We can expand the integrand in the above equation and obtain the following approximate expression for dimensionless perimeter

$$P^* \cong \frac{\pi}{32}(64+16M^2\varepsilon^2-3M^4\varepsilon^4) \tag{35}$$

Equation (35) along with Eq. (28) leads to the following expression for the dimensionless hydraulic diameter

$$D_h^* \cong \frac{128+64\varepsilon^2}{64+16M^2\varepsilon^2-3M^4\varepsilon^4} \tag{36}$$

B. Thermal Features

The energy equation for the thermally fully developed flow is given by

$$u\frac{\partial T}{\partial z} = \alpha\nabla^2 T \tag{37}$$

and the corresponding boundary conditions are written as

$$T \neq \infty \quad \text{at } r = 0 \tag{38}$$

$$T - T_w = \beta_t\lambda\frac{\partial T}{\partial n} \quad \text{at } r = R + R\varepsilon\sin(M\theta) \tag{39}$$

in which $\beta_t = [(2-F_t)/F_t][2\gamma/(1+\gamma)Pr]$. The usual way of modeling the thermally fully developed flow is to define the following dimensionless temperature which is independent of the axial direction

$$T^*(r,\theta) = \frac{T - T_w(z)}{\frac{q_{\mathrm{av}}R}{k}} \tag{40}$$

where $q_{\mathrm{av}} = \frac{\int q\,\mathrm{d}P}{P}$ is the average wall heat flux over the channel cross section. Taking differentiation of Eq. (40) with respect to z gives

$$\frac{\partial T}{\partial z} = \frac{\mathrm{d}T_w}{\mathrm{d}z} = \frac{\mathrm{d}T_b}{\mathrm{d}z} \tag{41}$$

with T_b being the bulk mean temperature. From an energy balance on a length of duct $\mathrm{d}z$, the following expression is obtained for $\mathrm{d}T_b/\mathrm{d}z$

$$\frac{\mathrm{d}T_b}{\mathrm{d}z} = \frac{q_{\mathrm{av}}P}{\rho c_p AU} \tag{42}$$

Since $\frac{\partial T}{\partial z}$ is constant, the axial conduction term in the energy equation will be zero. Therefore, the energy equation in dimensionless form may be written as

$$\nabla^{*2}T^* = \frac{\partial^2 T^*}{\partial r^{*2}} + \frac{1}{r^*}\frac{\partial T^*}{\partial r^*} + \frac{1}{r^{*2}}\frac{\partial^2 T^*}{\partial\theta^2} = \frac{4}{D_h^*}u^* \tag{43}$$

and the corresponding dimensionless boundary conditions are

$$T^* \neq \infty \quad \text{at } r^* = 0 \tag{44}$$

$$T^* = \beta_t Kn\frac{\partial T^*}{\partial n^*} \quad \text{at } r^* = 1+\varepsilon\sin(M\theta) \tag{45}$$

Similar to the velocity, the temperature is expanded as follows

$$T^*(r^*,\theta) = T_0^*(r^*,\theta) + \varepsilon T_1^*(r^*,\theta) + \varepsilon^2 T_2^*(r^*,\theta) + \cdots \tag{46}$$

which after substituting into Eq. (43) leads to the following equations

$$\nabla^{*2}T_0^* = \frac{4}{D_h^*}(a_0 + b_0 r^{*2}) \tag{47}$$

$$\nabla^{*2}T_1^* = \frac{4}{D_h^*}a_1 r^{*M}\sin(M\theta) \tag{48}$$

$$\nabla^{*2}T_2^* = \frac{4}{D_h^*}[a_2 + b_2 r^{*2M}\cos(2M\theta)] \tag{49}$$

A quick glance at both Eqs. (9) and (45) reveals that there is an analogy between the boundary condition at the wall for both dimensionless velocity and dimensionless temperature. Therefore, the boundary conditions for T_0^*, T_1^*, and T_2^* may be constructed from Eqs. (20–22) and the outcome is

$$T_0^*(1,\theta) = -\beta_t Kn\frac{\partial T_0^*}{\partial r^*}(1,\theta) \tag{50}$$

$$\begin{aligned} T_1^*(1,\theta) + \sin(M\theta)\frac{\partial T_0^*}{\partial r^*}(1,\theta) = -\beta_t Kn\Bigg[&\frac{\partial T_1^*}{\partial r^*}(1,\theta) \\ &+ \sin(M\theta)\frac{\partial^2 T_0^*}{\partial r^{*2}}(1,\theta) - M\cos(M\theta)\frac{\partial T_0^*}{\partial\theta}(1,\theta)\Bigg] \end{aligned} \tag{51}$$

$$\begin{aligned} &T_2^*(1,\theta) + \frac{M^2}{2}\cos^2(M\theta)T_0^*(1,\theta) \\ &\quad + \sin(M\theta)\frac{\partial T_1^*}{\partial r^*}(1,\theta) + \frac{\sin^2(M\theta)}{2}\frac{\partial^2 T_0^*}{\partial r^{*2}}(1,\theta) \\ &\quad = -\beta_t Kn\Bigg[\frac{\partial T_2^*}{\partial r^*}(1,\theta) + \sin(M\theta)\frac{\partial^2 T_1^*}{\partial r^{*2}}(1,\theta) \\ &\quad + \frac{\sin^2(M\theta)}{2}\frac{\partial^3 T_0^*}{\partial r^{*3}}(1,\theta) + 2M\sin(M\theta)\cos(M\theta)\frac{\partial T_0^*}{\partial\theta}(1,\theta) \\ &\quad - M\cos(M\theta)\frac{\partial T_1^*}{\partial\theta}(1,\theta) - M\sin(M\theta)\cos(M\theta)\frac{\partial^2 T_0^*}{\partial r^*\partial\theta}(1,\theta)\Bigg] \end{aligned} \tag{52}$$

The solutions of Eqs. (47–49) subject to boundary conditions (50–52) may be written as

$$T_0^* = A_0 + B_0 r^{*2} + C_0 r^{*4} \tag{53}$$

$$T_1^* = (A_1 r^{*M} + B_1 r^{*M+2}) \sin(M\theta) \tag{54}$$

$$T_2^* = A_2 + B_2 r^{*2} + (C_2 r^{*2M} + D_2 r^{*2M+2}) \cos(2M\theta) \tag{55}$$

where the coefficients are given below

$$A_0 = -\beta_t Kn\left(\frac{2a_0}{D_h^*} + \frac{b_0}{D_h^*}\right) - \frac{a_0}{D_h^*} - \frac{b_0}{4D_h^*}, \qquad B_0 = \frac{a_0}{D_h^*}$$

$$C_0 = \frac{b_0}{4D_h^*}$$

$$A_1 = -\frac{\beta_t Kn(\frac{M+2}{M+1}a_1 + 2a_0 + 3b_0) + 2a_0 + b_0 + \frac{a_1}{M+1}}{D_h^*(1 + \beta_t KnM)}$$

$$B_1 = \frac{a_1}{D_h^*(M+1)}$$

$$A_2 = -\frac{\beta_t Kn}{2}\left[M(M-1)A_1 + (M+2)(M+1)B_1 + 12C_0 - M^2(A_1 + B_1) + \frac{4a_2}{D_h^*}\right] - \frac{M^2}{4}(A_0 + B_0 + C_0) - \frac{1}{2}[MA_1 + (M+2)B_1] - \left(\frac{B_0}{2} + 3C_0\right) - \frac{a_2}{D_h^*}$$

$$B_2 = \frac{a_2}{D_h^*}, \qquad C_2 = \frac{\Lambda - \frac{b_2}{D_h^*(2M+1)}}{1 + 2\beta_t KnM}, \qquad D_2 = \frac{b_2}{D_h^*(2M+1)} \tag{56}$$

with

$$\Lambda = \frac{\beta_t Kn}{2}\left[M(M-1)A_1 + (M+2)(M+1)B_1 + 12C_0 + M^2(A_1 + B_1) - 4\frac{M+1}{2M+1}\frac{b_2}{D_h^*}\right] - \frac{M^2}{4}(A_0 + B_0 + C_0) + \frac{1}{2}[MA_1 + (M+2)B_1] + \frac{B_0}{2} + 3C_0 \tag{57}$$

Once the temperature distribution is obtained, the quantities of physical interest, including the bulk temperature of the fluid and the heat transfer rate can be obtained. The dimensionless bulk temperature is given by

$$T_b^* = \frac{M\int_0^{2\pi/M}\int_0^{1+\varepsilon\sin(M\theta)} u^* T^* r^* \,\mathrm{d}r^* \,\mathrm{d}\theta}{M\int_0^{2\pi/M}\int_0^{1+\varepsilon\sin(M\theta)} u^* r^* \,\mathrm{d}r^* \,\mathrm{d}\theta} = \frac{M}{\pi(1+\frac{\varepsilon^2}{2})}\int_0^{2\pi/M}\int_0^{1+\varepsilon\sin(M\theta)} u^* T^* r^* \,\mathrm{d}r^* \,\mathrm{d}\theta \tag{58}$$

After integration, the bulk temperature in dimensionless form becomes

$$T_b^* = \frac{a_0 A_b + b_0 B_b + a_1 C_b + a_2 D_b + O(\varepsilon^4)}{1 + \frac{\varepsilon^2}{2}} \tag{59}$$

with the following coefficients

$$A_b = A_0 + \frac{B_0}{2} + \frac{C_0}{3} + \left(\frac{A_0}{2} + \frac{3}{2}B_0 + \frac{5}{2}C_0 + A_1 + B_1 + A_2 + \frac{B_2}{2}\right)\varepsilon^2 + O(\varepsilon^4)$$

$$B_b = \frac{A_0}{2} + \frac{B_0}{3} + \frac{C_0}{4} + \left(\frac{3}{2}A_0 + \frac{5}{2}B_0 + \frac{7}{2}C_0 + A_1 + B_1 + \frac{A_2}{2} + \frac{B_2}{3}\right)\varepsilon^2 + O(\varepsilon^4)$$

$$C_b = \left[A_0 + B_0 + C_0 + \frac{A_1}{2(M+1)} + \frac{B_1}{2(M+2)}\right]\varepsilon^2 + O(\varepsilon^4)$$

$$D_b = \left(A_0 + \frac{B_0}{2} + \frac{C_0}{3}\right)\varepsilon^2 + O(\varepsilon^4) \tag{60}$$

Based on the definition, the Nusselt number is written as

$$Nu = \frac{hD_h}{k} = \frac{q_{\mathrm{av}} D_h}{k(T_w - T_b)} = -\frac{D_h^*}{T_b^*} \tag{61}$$

IV. Method Validation

First of all, it is convenient to examine the accuracy of the suggested expression for dimensionless hydraulic diameter, i.e., Eq. (36), as it is essential in expressing both friction factor and Nusselt number. For this purpose, the integral of Eq. (34) was performed numerically using both MAPLE and MATLAB solvers as well as an in-house code. The results of both softwares and the in-house code were found to be identical up to four decimal digits. The numerical results along with those predicted by the approximate expression (36) are presented in Table 1. One can see that the approximate expression can well predict the hydraulic diameter. The error incurred by using the approximate expression increases with increasing values of M and ε and reaches about 0.2% for $M = 12$ and $\varepsilon = 0.06$. Despite the good agreement between the results, unfortunately our results do not coincide with corresponding values supplied by Shah and London [37] at higher values of M and ε.

Tables 2 and 3 compare the values of Poiseuille number and Nusselt number, respectively, for the special case of no slip conditions, i.e., $Kn = 0$. It is worth mentioning that we use $Kn = 0$ to indicate the no slip limit at which the Knudsen number is so small that the slip velocity is negligible compared with the velocity scale of the problem. Hence in the rest of the paper $Kn = 0$ indicates a limit that $Kn \to 0$ but never $Kn \equiv 0$. As seen, when the value of D_h^* from Shah and London [37] is used to calculate the Poiseuille and Nusselt numbers, the present results are in good agreement with their reported ones. The Poiseuille numbers calculated based on the hydraulic diameters reported by [37] are also in excellent agreement with those reported by Duan and Muzychka [35]. This is not surprising, because they used the values of hydraulic diameter from the same reference. It is worth noting that for the special case of a smooth pipe, i.e., $\varepsilon = 0$, our expression for Nusselt number and the one given by Ameel et al. [40] predict identical values.

Table 1 Comparison of the values of $D_h^*/2$

		$D_h^*/2$		
M	ε	Present work		
		Numerical	Approximate	Shah and London [37]
6	0.02	0.9966	0.9966	0.9966
	0.04	0.9867	0.9867	0.9863
	0.06	0.9710	0.9711	0.9689
8	0.02	0.9939	0.9939	0.9938
	0.04	0.9763	0.9763	0.9747
	0.06	0.9492	0.9495	0.9418
12	0.02	0.9861	0.9862	0.9856
	0.04	0.9483	0.9485	0.9402
	0.06	0.8951	0.8969	0.8583

Table 2 Comparison between the values of Poiseuille number obtained in the present study for no slip conditions and those reported by [35,37]

		fRe			
M	ε	Present work			
		D_h^* from Eq. (36)	D_h^* from [37]	Duan and Muzychka [35]	Shah and London [37]
6	0.02	15.9527	15.9520	15.952	15.952
	0.04	15.8189	15.8046	15.805	15.806
	0.06	15.6219	15.5512	15.551	15.559
8	0.02	15.8902	15.8880	15.888	15.887
	0.04	15.5866	15.5359	15.536	15.542
	0.06	15.1594	14.9154	14.915	14.943
12	0.02	15.6949	15.6773	15.677	15.679
	0.04	14.9076	14.6471	14.647	14.671
	0.06	13.9474	12.7738	12.774	12.872

Table 3 Comparison between the values of Nusselt number obtained in the present study for no slip conditions and those reported by [37]

		Nu		
M	ε	Present work		
		D_h^* from Eq. (36)	D_h^* from [37]	Shah and London [37]
6	0.02	4.3401	4.3399	4.340
	0.04	4.2731	4.2693	4.267
	0.06	4.1737	4.1548	4.142
8	0.02	4.3167	4.3161	4.316
	0.04	4.1864	4.1728	4.168
	0.06	4.0016	3.9371	3.912
12	0.02	4.2507	4.2460	4.245
	0.04	3.9575	3.8884	3.875
	0.06	3.5946	3.2921	3.231

V. Results and Discussion

In presenting the results, it is assumed that the values of accommodation coefficients are equal to unity. Also the values of Prandtl number and the heat capacity ratio are set to be 0.7 and 1.4, respectively. Based on these assumptions, the friction factor and Nusselt number will be dependent on three parameters comprising Knudsen number, relative roughness, and the number of corrugations. First of all, it is convenient to inspect the effects of roughness on the hydrodynamic features.

The dimensionless velocity profile at different Knudsen numbers for $M = 10$ and $\varepsilon = 0.03$ at the angular position of $\theta = \pi/2M$ is illustrated in Fig. 2. As a result of slip conditions, slip velocities occur at the wall for non zero values of Kn. An increase in Kn results in an increase in the slip velocity at the wall, while according to mass conservation, the maximum velocity decreases. Note that as Knudsen number increases the velocity gradient becomes smaller, especially at the wall at which the maximum decrease occurs. We will see that this leads to decreasing the pressure drop for higher Knudsen numbers.

Figure 3 shows the velocity profile at different angular positions for $M = 10$ and $Kn = 0.05$. In the presence of roughness, the change of velocity profile relative to that for smooth channel is quite different for concave $(0 < \theta < \pi/M)$ and convex $(\pi/M < \theta < 2\pi/M)$ regions. In the concave region, which is represented by $\theta = \pi/2M$, the effect of roughness is to decrease dimensionless velocity over the majority of the channel cross section, while, according to mass conservation, it is to increase velocity in the convex region represented by $\theta = 3\pi/2M$. Away from the wall, both profiles merge with each other due to decadence of the wall corrugation effects.

The graphs of the pressure gradient versus M at different values of Knudsen number and relative roughness while keeping $\pi R^4/\mu Q = 1$ are illustrated in Fig. 4. As expected, increasing Knudsen number decreases the pressure drop. This is due to the fact that rarefaction decreases momentum exchange between the fluid and the solid surface. In other words, the fluid less senses the presence of the wall. The pressure drop increases as the relative roughness or the number of corrugations increase. The quantitative value of the increase in the pressure drop at $\varepsilon = 0.05$ and $Kn = 0.05$, relative to the smooth tube, is about 12.3% for $M = 25$. Increasing pressure drop arising from increasing values of the relative roughness, which is consistent with the results of Sun and Faghri [34], is mainly due to increasing the ratio of the channel surface to the channel area.

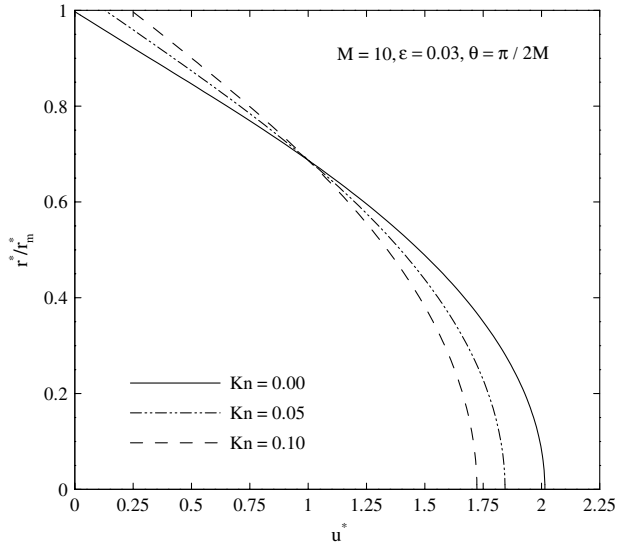

Fig. 2 Dimensionless velocity profile at different Knudsen numbers.

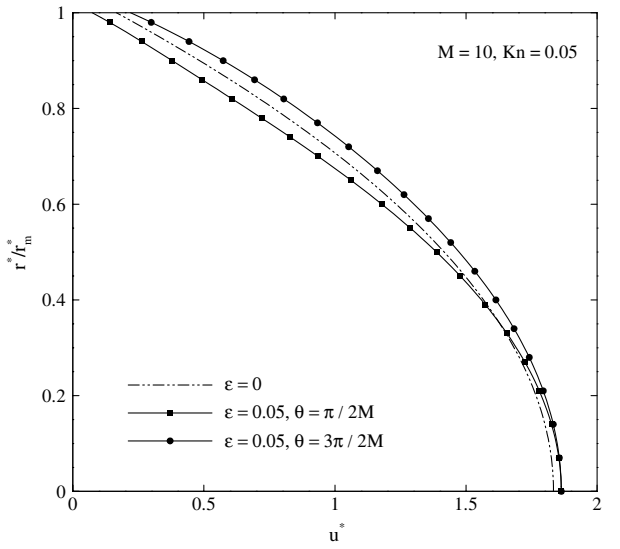

Fig. 3 Dimensionless velocity profile at different angular positions.

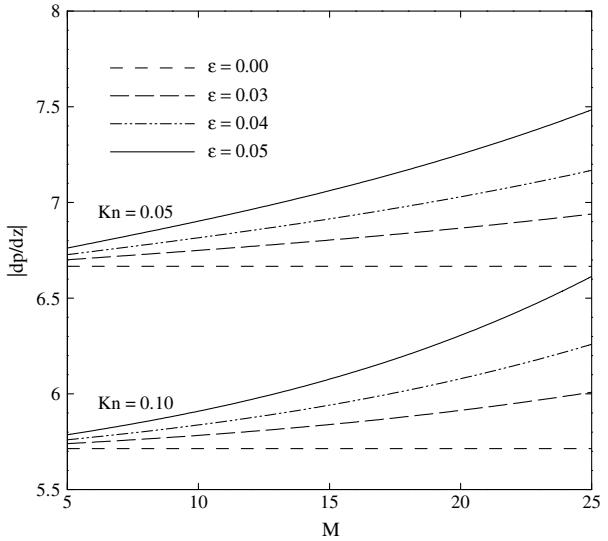

Fig. 4 Pressure gradient vs M at different values of Knudsen number and relative roughness while keeping $\pi R^4/\mu Q = 1$.

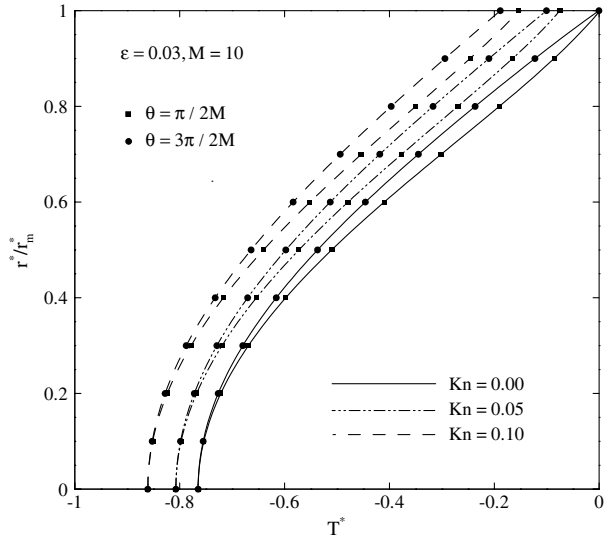

Fig. 6 Radial distribution of dimensionless temperature at different values of angular position and Knudsen number.

Figure 5 exhibits the radial distribution of dimensionless temperature at different angular positions for $M = 10$ and $Kn = 0.05$. It can be seen that, in the convex region, smaller values of dimensionless temperature compared with that for the smooth tube are obtained which means that the temperature difference between the fluid particles and the wall increases. In the concave region, two different behaviors are observed, namely increasing the dimensionless temperature in the region adjacent to the wall and decreasing it in the core region. These trends may be interpreted using the velocity profiles given by Fig. 3. A decrease in velocity gives the fluid particles the opportunity to sense the wall effects more by means of the thermal energy diffusion. In the concave region, the velocity of the near wall region decreases, leading to a more effect of thermal diffusion, and consequently, a smaller temperature difference between the fluid particles and the solid surface. The opposite of the aforementioned description is right for the core region.

The radial distribution of dimensionless temperature at different values of the angular position and the Knudsen number is presented in Fig. 6. As observed, an increase in the effect of rarefaction leads to a greater difference between the fluid and wall temperatures which is mainly due to the temperature jump at the wall. For all the Knudsen numbers, the temperature gradient at the wall in the convex region is higher than that in the concave region which means that the local wall heat flux is greater in the convex region.

The main theme of the present work is to study heat transfer rates which may be expressed in terms of the Nusselt number. Figure 7 demonstrates the Nusselt number values as a function of M at different values of the Knudsen number and the relative roughness. The Nusselt number decreases as the Knudsen number increases, which is an expected trend arising from the fact that rarefaction decreases heat transfer rates. The Nusselt number also decreases as the relative roughness or the number of corrugations increase. The effect of the relative roughness on the Nusselt number is more pronounced at higher values of M. Decreasing Nusselt number with increasing values of the relative roughness can be explained by means of Fig. 5. Although in the vicinity of the surface of the concave region, smaller temperatures with negative sign compared with the smooth tube are obtained, however, regarding the variations of the velocity profile, it may be concluded that for a higher value of relative roughness, the bulk temperature takes higher values with negative sign. Therefore, according to Eq. (61), smaller values of Nusselt number are obtained.

Besides the Nusselt number, it is convenient to study the variations of the heat transfer rate per unit length of the channel, i.e., $Q' =$

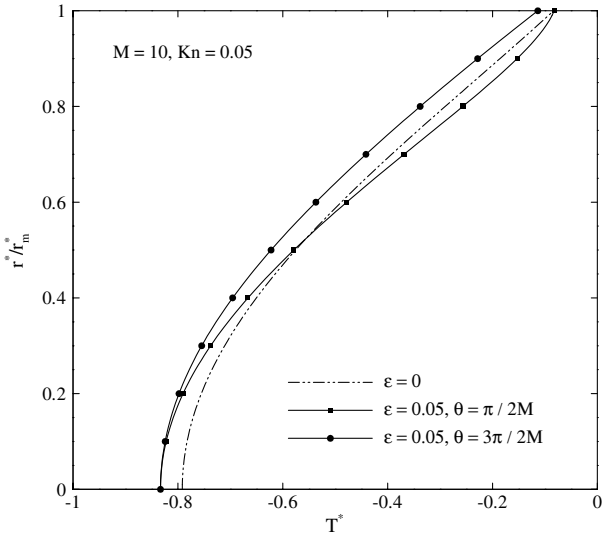

Fig. 5 Radial distribution of dimensionless temperature at different angular positions.

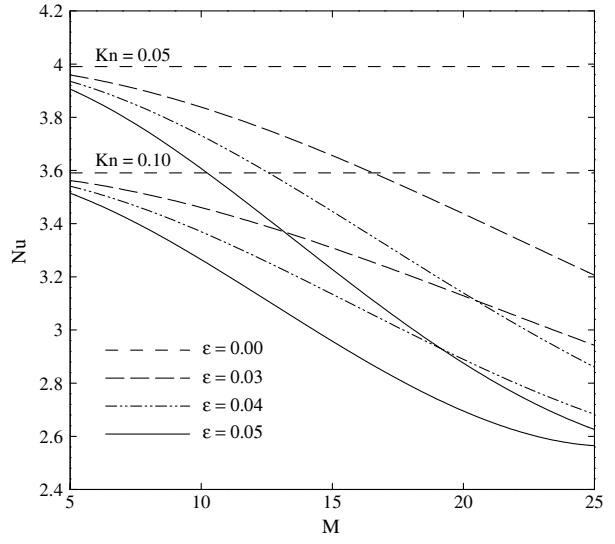

Fig. 7 Nusselt number vs M at different values of Knudsen number and relative roughness.

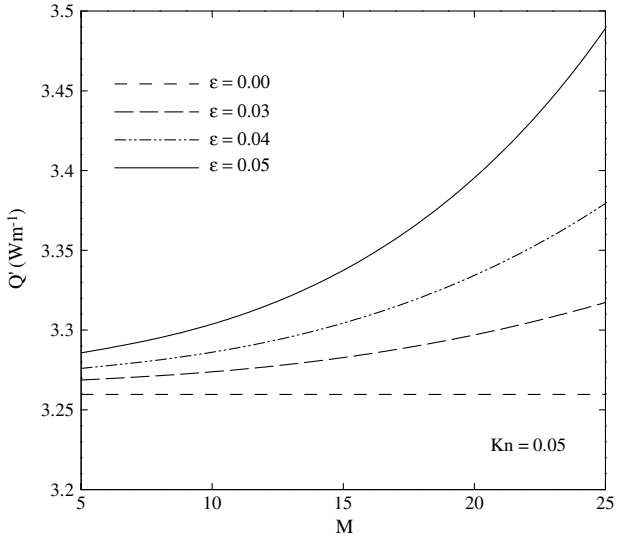

Fig. 8 Heat transfer rate per unit length for air vs M at different values of relative roughness for a nominal radius of $R = 2\ \mu$m and $T_w - T_b = 10$ K.

$hP(T_w - T_b)$ which is shown in Fig. 8. The value of thermal conductivity is assumed to be $k = 0.026$ Wm^{-1} K^{-1}, the air thermal conductivity at standard atmospheric conditions. Moreover, a nominal channel radius of $R = 2\ \mu$m is considered to yield a Knudsen number of 0.05 for a mean free path of about 100 nm. The temperature difference between the wall and the bulk fluid is set to be 10 K. As observed, the heat transfer rate increases as the relative roughness or the number of corrugations increases. This behavior, which is consistent with the experimental results of Wu and Cheng [31], is the result of increasing the channel surface giving the fluid more of an opportunity to transfer additional heat. The quantitative value of the increase in the heat transfer rate at $\varepsilon = 0.05$, compared with the smooth tube, is about 7.0% for $M = 25$. It was found previously that the corresponding value of the increase in the pressure drop is about 12.3%. Therefore, the channel performance, defined as $\eta = Q'/(\mathrm{d}p/\mathrm{d}z)$, for $\varepsilon = 0.05$ is about 4.7% smaller than that for smooth pipe which means that for a given value of the heat transfer rate we incur some increase in pumping power requirements. In other words, this is to say that the corrugated roughness, in spite of increasing the capacity of heat transfer, leads to a little decrease in the channel performance and therefore is an undesirable phenomenon. The channel performance as a function of M at different values of the relative roughness is shown in Fig. 9. As mentioned previously, the performance is decreased with increasing values of the relative roughness. The effect of roughness is more pronounced at higher values of M.

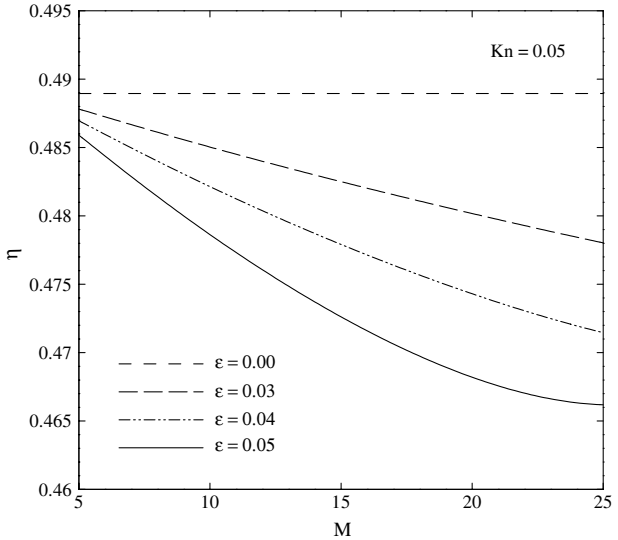

Fig. 9 Channel performance as a function of M at different values of the relative roughness.

VI. Conclusions

The effect of corrugated roughness on the fully developed forced convection of a rarefied gas in a micropipe was investigated in this work. The rarefaction effects were treated using first-order slip velocity and temperature jump boundary conditions. The governing equations were solved by means of the straightforward perturbation method. Closed-form solutions were obtained for the dimensionless velocity and temperature distributions, for the friction coefficient and pressure drop, and finally for the Nusselt number. The effects of roughness on the flow parameters were discussed in detail. The results confirmed the previous works' conclusions that the pressure drop is an increasing function of the relative roughness. It was also found that although the Nusselt number decreases with increasing roughness, roughness leads to a higher rate of heat transfer. Despite increasing the heat transfer rate, the effect of roughness was found to be unfavorable as it leads to more increase of the pressure drop leading to smaller values of the channel performance.

References

[1] Harley, J., Huang, Y., Bau, H., and Zemel, J. N., "Gas Flow in Microchannels," *Journal of Fluid Mechanics*, Vol. 284, 1995, pp. 257–274.
doi:10.1017/S0022112095000358

[2] Araki, T., Kim, M. S., Hiroshi, I., and Suzuki, K., "An Experimental Investigation of Gaseous Flow Characteristics in Microchannels," *Microscale Thermophysical Engineering*, Vol. 6, No. 2, 2002, pp. 117–130.
doi:10.1080/10893950252901268

[3] Arkilic, E. B., Breuer, K. S., and Schmidt, M. A., "Gaseous Slip Flow in Long Microchannels," *Journal of Microelectromechanical Systems*, Vol. 6, No. 2, 1997, pp. 167–178.
doi:10.1109/84.585795

[4] Arkilic, E. B., Breuer, K. S., and Schmidt, M. A., "Mass Flow and Tangential Momentum Accommodation in Silicon Micromachined Channels," *Journal of Fluid Mechanics*, Vol. 437, 2001, pp. 29–43.
doi:10.1017/S0022112001004128

[5] Liu, J., Tai, Y. C., and Ho, C. M., "MEMS for Pressure Distribution Studies of Gaseous Flows in Microchannels," *Proceedings of IEEE, International Conference on Micro Electro Mechanical Systems*, IEEE Publications, Piscataway, NJ, 1995, pp. 209–215.

[6] Choi, S. B., Barron, R. F., and Warrington, R. O., "Fluid Flow and Heat Transfer in Microtubes," *Proceedings of Micromechanical Sensors, Actuators, and Systems*, Vol. 32, ASME, Fairfield, NJ, 1991, pp. 123–134.

[7] Taheri, P., Torrilhon, M., and Struchtrup, H., "Couette and Poiseuille Microflows: Analytical Solutions for Regularized 13-Moment Equations," *Physics of Fluids*, Vol. 21, No. 1, 2009, p. 017102.
doi:10.1063/1.3064123

[8] Beskok, A., and Karniadakis, G. E., "Simulation of Heat and Momentum Transfer in Complex Micro-Geometries," *Journal of Thermophysics and Heat Transfer*, Vol. 8, No. 4, 1994, pp. 647–655.
doi:10.2514/3.594

[9] Hadjiconstantinou, N. G., "The Limits of Navier–Stokes Theory and Kinetic Extensions for Describing Small Scale Gaseous Hydrodynamics," *Physics of Fluids*, Vol. 18, No. 11, 2006, p. 111301.
doi:10.1063/1.2393436

[10] Kennard, E. H., *Kinetic Theory of Gases*, McGraw–Hill, New York, 1938.

[11] Ebert, W. A., and Sparrow, E. M., "Slip Flow in Rectangular and Annular Ducts," *Journal of Basic Engineering*, Vol. 87, No. , 1965, pp. 1018–1024.

[12] Duan, Z., and Muzychka, Y. S., "Slip Flow in Elliptic Microchannels," *International Journal of Thermal Sciences*, Vol. 46, No. 11, 2007, pp. 1104–1111.
doi:10.1016/j.ijthermalsci.2007.01.026

[13] Duan, Z., and Muzychka, Y. S., "Slip Flow in Non-Circular Microchannels," *Microfluids and Nanofluids*, Vol. 3, No. 4, 2007, pp. 473–484.
doi:10.1007/s10404-006-0141-4

[14] Duan, Z., and Muzychka, Y. S., "Slip Flow in the Hydrodynamic Entrance Region of Circular and Noncircular Microchannels," *Journal of Fluids Engineering*, Vol. 132, No. 1, 2010, p. 011201. doi:10.1115/1.4000692

[15] Aydin, O., and Avci, M., "Heat and Flow Characteristics of Gases in Micropipes," *International Journal of Heat and Mass Transfer*, Vol. 49, Nos. 9–10, 2006, pp. 1723–1730. doi:10.1016/j.ijheatmasstransfer.2005.10.020

[16] Aydin, O., and Avci, M., "Analysis of Laminar Heat Transfer in Micro-Poiseuille Flow," *International Journal of Thermal Sciences*, Vol. 46, No. 1, 2007, pp. 30–37. doi:10.1016/j.ijthermalsci.2006.04.003

[17] Jeong, H. E., and Jeong, J. T., "Extended Graetz Problem Including Axial Conduction and Viscous Dissipation in Microtube," *Journal of Mechanical Science and Technology*, Vol. 20, No. 1, 2006, pp. 158–166. doi:10.1007/BF02916209

[18] Jeong, H. E., and Jeong, J. T., "Extended Graetz Problem Including Streamwise Conduction and Viscous Dissipation in Microchannel," *International Journal of Heat and Mass Transfer*, Vol. 49, Nos. 13–14, 2006, pp. 2151–2157. doi:10.1016/j.ijheatmasstransfer.2005.11.026

[19] Sadeghi, A., Asgarshamsi, A., and Saidi, M. H., "Analysis of Laminar Flow in the Entrance Region of Parallel Plate Microchannels for Slip Flow," *Proceedings of the Seventh International ASME Conference on Nanochannels, Microchannels and Minichannels, ICNMM2009*, ASME, Fairfield, NJ, 2009.

[20] Tunc, G., and Bayazitoglu, Y., "Heat Transfer in Rectangular Microchannels," *International Journal of Heat and Mass Transfer*, Vol. 45, No. 4, 2002, pp. 765–773. doi:10.1016/S0017-9310(01)00201-0

[21] Yu, S., and Ameel, T. A., "Slip Flow Heat Transfer in Rectangular Microchannels," *International Journal of Heat and Mass Transfer*, Vol. 44, No. 22, 2001, pp. 4225–4234. doi:10.1016/S0017-9310(01)00075-8

[22] Yu, S., and Ameel, T. A., "Slip Flow Convection in Isoflux Rectangular Microchannels," *Journal of Heat Transfer*, Vol. 124, No. 2, 2002, pp. 346–355. doi:10.1115/1.1447932

[23] Naterer, G. F., "Adaptive Surface Microprofiling for Microfluidic Energy Conversion," *Journal of Thermophysics and Heat Transfer*, Vol. 18, No. 4, 2004, pp. 494–501. doi:10.2514/1.8728

[24] Khan, A. W., and Yovanovich, M. M., "Analytical Modeling of Fluid Flow and Heat Transfer in Microchannel/Nanochannel Heat Sinks," *Journal of Thermophysics and Heat Transfer*, Vol. 22, No. 3, 2008, pp. 352–359. doi:10.2514/1.35621

[25] Sadeghi, A., and Saidi, M. H., "Viscous Dissipation and Rarefaction Effects on Laminar Forced Convection in Microchannels," *Journal of Heat Transfer*, Vol. 132, No. 7, 2010, p. 072401. doi:10.1115/1.4001100

[26] Sadeghi, A., and Saidi, M. H., "Second Law Analysis of Slip Flow Forced Convection Through a Parallel Plate Microchannel," *Nanoscale and Microscale Thermophysical Engineering*, Vol. 14, No. 4, 2010, pp. 209–228. doi:10.1080/15567265.2010.502924

[27] Sadeghi, A., Asgarshamsi, A., and Saidi, M. H., "Thermodynamic Analysis of Slip Flow Forced Convection Through a Microannulus," *Journal of Thermophysics and Heat Transfer*, Vol. 24, No. 4, 2010, pp. 785–795. doi:10.2514/1.48036

[28] Kandlikar, S. G., Garimella, S., Li, D., Colin, S., and King, M. R., *Heat Transfer and Fluid Flow in Minichannels and Microchannels*, Elsevier, Oxford, 2006.

[29] Peng, X. F., Peterson, G. P., and Wang, B. X., "Frictional Flow Characteristics of Water Flowing Through Rectangular Microchannels," *Experimental Heat Transfer*, Vol. 7, No. 4, 1994, pp. 249–264.

[30] Mala, G. M., and Li, D., "Flow Characteristics of Water in Microtubes," *International Journal of Heat and Fluid Flow*, Vol. 20, No. 2, 1999, pp. 142–148. doi:10.1016/S0142-727X(98)10043-7

[31] Wu, H. Y., and Cheng, P., "An Experimental Study of Convective Heat Transfer in Silicon Microchannels with Different Surface Conditions," *International Journal of Heat and Mass Transfer*, Vol. 46, No. 14, 2003, pp. 2547–2556. doi:10.1016/S0017-9310(03)00035-8

[32] Kandlikar, S. G., Schmitt, D., Carrano, A. L., and Taylor, J. B., "Characterization of Surface Roughness Effects on Pressure Drop in Single-Phase Flow in Minichannels," *Physics of Fluids*, Vol. 17, No. 10, 2005, p. 100606. doi:10.1063/1.1896985

[33] Li, W. L., Lin, J. W., Lee, S. C., and Chen, M. D., "Effects of Roughness on Rarefied Gas Flow in Long Microtubes," *Journal of Micromechanics and Microengineering*, Vol. 12, No. 2, 2002, pp. 149–156. doi:10.1088/0960-1317/12/2/308

[34] Sun, H., and Faghri, M., "Effects of Surface Roughness on Nitrogen Flow in a Microchannel Using the Direct Simulation Monte Carlo Method," *Numerical Heat Transfer*, Vol. 43, No. 1, 2003, pp. 1–8. doi:10.1080/10407780307302

[35] Duan, Z., and Muzychka, Y. S., "Effects of Corrugated Roughness on Developed Laminar Flow in Microtubes," *Journal of Fluids Engineering*, Vol. 130, No. 3, 2008, p. 031102. doi:10.1115/1.2842148

[36] Duan, Z., and Muzychka, Y. S., "Effects of Axial Corrugated Roughness on Low Reynolds Number Slip Flow and Continuum Flow in Microtubes," *Journal of Heat Transfer*, Vol. 132, No. 4, 2010, p. 041001. doi:10.1115/1.3211854

[37] Shah, R. K., and London, A. L., *Laminar Flow Forced Convection in Ducts*, Academic Press, New York, 1978.

[38] Beskok, A., Karniadakis, G. E., and Trimmer, W., "Rarefaction and Compressibility Effects in Gas Microflows," *Journal of Fluids Engineering*, Vol. 118, No. 3, 1996, pp. 448–456. doi:10.1115/1.2817779

[39] Schaaf, S. A., "Mechanics of Rarefied Gases," *Encyclopedia of Physics*, Vol. 8.22, Springer, Berlin, 1963, pp. 591–624.

[40] Ameel, T. A., Wang, X. M., Baron, R. F., and Warrington, R. O., "Laminar Forced Convection in a Circular Tube with Constant Heat Flux and Slip Flow," *Microscale Thermophysical Engineering*, Vol. 1, No. 4, 1997, pp. 303–320. doi:10.1080/108939597200160